

Non-Orthogonal Multiple Access for UAV-Aided Heterogeneous Networks: A Stochastic Geometry Model

Cunzhuo Zhao, Yuanwei Liu, Yunlong Cai, and Minjian Zhao

Abstract

The potential benefits of deploying unmanned aerial vehicles (UAVs) as aerial base stations (ABSs) with sub-6GHz band and small cells terrestrial base stations (TBSs) with millimeter wave (mmWave) band in a hybrid heterogeneous networks (HetNets) is explored. A flexible non-orthogonal multiple access (NOMA) based user association policy is proposed. By using the tools from stochastic geometry, new analytical expressions for association probability, coverage probability and spectrum efficiency are derived for characterizing the performance of UAV-aided HetNets under the realistic Air-to-Ground (A2G) and Ground-to-Ground (G2G) channels. Finally, we provide insights on the proposed hybrid HetNets by numerical results. We confirm that i) the proposed NOMA enabled HetNets is capable of achieving superior performance compared with the OMA enabled ABSs by setting power allocation factors and targeted signal-to-interference-plus-noise ratio (SINR) threshold properly; ii) there is a tradeoff between the association probabilities and the spectrum efficiency in the NOMA enabled ABSs tier; iii) compared with sub-6GHz ABSs, mmWave enabled TBSs are capable of enhancing the spectrum efficiency when the mmwave line-of-sight (LoS) link is available.

Index Terms

HetNets, mmWave, NOMA, stochastic geometry, UAV.

I. INTRODUCTION

In recent years, unmanned aerial vehicles (UAVs), commonly known as drones, have become a hotspot for wireless communications due to its unique attributes such as low-cost, mobility, and flexible reconfiguration [1]. In the meantime, in the process of standardization for 5G/B5G networks, UAVs are gradually being considered as an critical candidate to support diverse

C. Zhao, Y. Cai and M. Zhao are with the College of Information Science and Electronic Engineering, Zhejiang University, Hangzhou 310027, China (Email: zhaocz@zju.edu.cn; ylcai@zju.edu.cn; mjzhao@zju.edu.cn).

Y. Liu is with the School of Electronic Engineering and Computer Science, Queen Mary University of London, London E1 4NS, U.K. (Email: yuanwei.liu@qmul.ac.uk).

applications, such as reconnaissance, remote sensing, or working as temporal base stations [2]. The popularity of UAVs motivates the researchers to explore the opportunities for integrating UAVs into the existing wireless networks.

In the existing wireless networks, it is difficult to achieve universal connectivity due to the severe path loss and excessive inter-cell interference. One efficient approach to improve the coverage in currently deployed terrestrial cellular networks is to equip the UAVs as aerial base stations (ABS), augmented with the functionalities of terrestrial base stations (TBSs) [3]. As compared to terrestrial cellular networks, one distinct feature of UAV communications is that the Air-to-Ground (A2G) links are more likely to experience line-of-sight (LoS) propagation which offers lower attenuation [4]. To further exploit the spectrum efficiency of the UAV-aided networks, non-orthogonal multiple access (NOMA) has attracted much attention for its capability of serving multiple user equipments (UEs) at different quality-of-service (QoS) requirements in the same resource block [5], [6]. The key idea of NOMA is to employ a superposition coding (SC) at the transmitter and successive interference cancellation (SIC) at the receiver [7], which provides a good trade-off between the throughput of the system and the UEs fairness. Therefore, by adopting NOMA techniques, the achievable spectrum efficiency of the networks can be improved.

On the other hand, using high-frequency band and densification will be two key capacity-increasing techniques for cellular networks, such as millimeter wave (mmWave) communications [8] and small cells. Deploying terrestrial mmWave small cells will offer high capacity when a connection is available. Motivated by the benefits of UAV-aided networks, NOMA techniques, and mmWave transmissions, in this work we consider a UAV-aided heterogeneous network (HetNets) where a mmWave terrestrial network co-exists with a sub-6GHz NOMA enabled aerial network. Note that the use of mmWave and microWave resources simultaneously is a feature of 5G/B5G networks, and their distinctive carrier frequencies avoid the inter-tier interference [9].

A. Related Work and Motivation

Modeling and analyzing cellular networks with the aid of stochastic geometry has been widely adopted due to its accuracy and tractability. In the studies of UAV-aided networks, the authors of [10] derived the coverage probability for a finite ABS network by modeling the locations of ABSs as a uniform binomial point process (BPP). The authors [11] analyzed the downlink coverage

performance of UAV-aided cellular networks when the UEs are clustered around the projections of ABSs on the ground. A framework was proposed in [12] to analyze the behaviors of a ABSs network under a realistic A2G channel model which incorporates the LoS and non-line-of-sight (NLoS) links. This work was further extended in [13] where the network comprises both ABSs and TBSs. Besides, instead of considering the average probabilistic path loss in most of works, the authors of [12], [13] considered more realistic LoS and NLoS transmissions, respectively. Multi-tier UAV-aided networks were presented in [3], [14], [15]. Specifically, the authors of [3] and [14] proposed the multi-tier drone architecture based on the standard terrestrial path loss model. Furthermore, the multi-tier UAV-aided networks based on the transmitter-oriented or receiver-oriented rules under a realistic A2G channel model were studied in [15]. The authors of [16] advocated a pair of strategies in UAV-aided NOMA networks, i.e., the UAV-centric strategy for offloading actions and the user-centric strategy for providing emergency communications. In [17], a multiple-input multiple-output (MIMO)-NOMA enabled UAV network was proposed, where the outage probability and ergodic rate were evaluated in the downlink scenario.

Regarding the literature of stochastic geometry based HetNets systems, a system containing sub-6GHz macrocells and mmWave small cells was analyzed in [18], where the macrocells provide universal coverage and the small cells provide high data rate when the mmWave LoS link is available. The authors of [19] studied the decoupled association in a sub-6GHz and mmWave deployment from the resource allocation perspective. Building upon the above research contributions and the analytical tools of stochastic geometry, we propose an architecture of UAV-aided HetNets where mmWave terrestrial networks co-exist with a sub-6GHz aerial networks, which has not been well studied in the literature. In contrast to the previously reported designs of UAV-aided HetNets [13], [15], our proposed architecture poses three additional challenges: i) The NOMA techniques causes additional interference from the connected ABS to the served UE; ii) The channel ordering needs to be determined under the unique characteristics of A2G channels; iii) The UE association policy needs to be carefully designed under the existence of mmWave TBSs and sub-6GHz ABSs.

B. Contributions and Organization

The primary contributions of this paper can be summarized as follows:

- By taking advantage of unique attributes of UAVs and high transmission rate of mmWave, we propose a new model of HetNets where the sub-6GHz NOMA enabled ABSs overlay the mmWave TBSs. We model the Ground-to-Ground (G2G) and A2G links incorporating the impact of LoS and NLoS path loss attenuations. We consider the LoS and NLoS transmissions separately, where two independent non-homogeneous poisson point processes (PPPs) are formulated.
- We develop a flexible association policy to address the co-existence of NOMA enabled ABSs and mmWave TBSs. Under this policy, we first derive the analytical expressions for the distance distributions given that the typical UE is associated with a TBS, a NLoS ABS or a LoS ABS.
- We derive exact analytical expressions for the UAV-aided HetNets in terms of coverage probability and spectrum efficiency. Additionally, the closed-form coverage probability expressions are obtained in mmWave tier.
- We provide the basic power allocation guidelines for the NOMA enabled networks, in which the targeted signal-to-interference-plus-noise ratio (SINR) threshold of the typical UE and the fixed UE both determine the coverage probability of a typical UE. We also provide insights on the HetNets design by numerical results, which demonstrate that our proposed NOMA enabled HetNets is capable of achieving superior performance compared with the conventional OMA enabled HetNets.

The rest of this paper is organized as follows. In Section II, the HetNets model and the association strategy are introduced. In Section III, new analytical expressions for distance distributions and association probabilities are derived. Then the coverage probability and spectrum efficiency of the network are investigated in Section IV and Section V, respectively. Our numerical results are demonstrated in Section VI, which is followed by the conclusions in Section VII.

II. NETWORK MODEL

A. Network Description

In this work, we present a two tier downlink UAV-aided hybrid HetNets system shown in Fig. 1. In tier 1, the TBSs provide wireless connectivity to the ground UEs, where the spatial distribution of TBSs is modeled as an HPPP Φ_T with density λ_T . In tier 2, the ABSs are deployed

to enhance the coverage or boost the capacity. We assume that all the ABSs hover at a height h and their horizontal locations form an HPPP Φ_A with density λ_A . It is worth mentioning that the analysis in this network model is also applicable for the ABSs with different altitudes [10]. Specially, in tier 1 the TBSs are equipped with multiple antennas and the mmWave band is utilized to provide fast data rate in short-range small cells, while in tier 2 the ABSs adopt sub-6GHz and NOMA techniques in order to improve the coverage and freedom to serve multiple UEs. All the UEs are assumed to be equipped with a single antenna. Without loss of generality, the analysis is conducted based on a typical UE positioned at the origin. All the symbol notations are list in Table I.

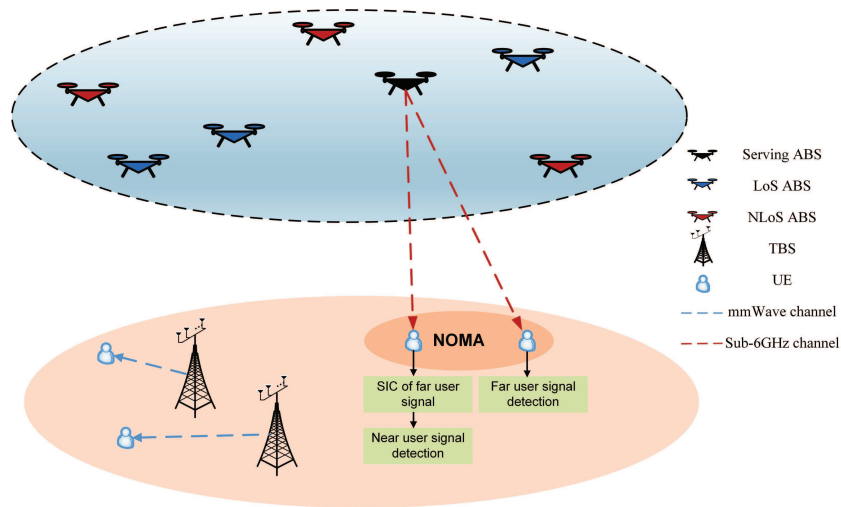


Fig. 1: Illustration of UAV-aided hybrid HetNets.

B. Channel Characteristics and Directional Beamforming in mmWave tier

In the first tier of the networks, due to the deployment of mmWave, the transmitted signals suffer from attenuation due to the obstacles, and the blockage effect can not be neglected. Here we adopt a tractable equivalent LoS ball model [20] to characterize the blockage effect, which enables fast numerical computation and simplifies the analysis. We define a LoS radius R_B , which represents the maximum distance between a UE and its potential mmWave TBS, and the LoS probability is one within R_B and zero outside this radius. It has been shown that the LoS ball model can fit the real environment properly and provide enough analytical accuracy compared with other blockage models [20]. Regarding the NLoS paths, it has been pointed out in [21] that the impact of NLoS signals and NLoS interference can be ignored in mmWave networks.

TABLE I: Table of Notations

Notation	Description
Φ_T, Φ_A	HPPP of TBSs with density λ_T , HPPP of ABSs with density λ_A
Φ_L, Φ_N	PPP of LoS ABSs with density λ_A , PPP of NLoS ABSs with density λ_A
a, b	S-curve parameters
$P_L(x), P_N(x)$	Probability of LoS/NLoS links under the horizontal distance x
R_B, h, R_f	mmWave LoS radius, ABS height, fixed UE distance
$R_{N,0}, R_{L,0}, R_{T,0}$	Minimum distance between the typical UE and the NLoS ABSs, LoS ABSs and TBSs
$\alpha_N, \alpha_L, \alpha_T$	Path loss exponent between the typical UE and NLoS ABS, LoS ABS and TBS
C_N, C_L, C_T	Additive loss exponent between the typical UE and NLoS ABS, LoS ABS and TBS
m_N, m_L, m_T	Nakagami- m fading parameters between the typical UE and NLoS ABS, LoS ABS and TBS
a_m, a_n	NOMA coefficients
P_T, P_A, σ^2	TBS transmit power, ABS transmit power, noise power

Hence, we will focus on the analysis where the typical UE is associated with a LoS TBS. Then the process for the case the TBSs located inside the LoS Ball $\mathcal{B}(0, R_B)$ can be expressed as $\Phi_T \cap \mathcal{B}(0, R_B)$. As a result, the path loss in the TBS tier can be expressed as

$$L_T(r) = \mathbf{1}(R_B - r)C_T r^{-\alpha_T}, \quad (1)$$

where r is the communication distance, $\mathbf{1}(x)$ is the unit step function, C_T and α_T are the additive loss and path loss exponents, respectively. We also characterize the small scale fading with the Nakagami- m fading, where the channel gain follows the Gamma distribution with parameter $\Gamma(m_T, \frac{1}{m_T})$.

In this work, multiple antennas are equipped at the TBSs to accomplish the directional beamforming, and we adopt a 3D sectorized model [22], [23]. The directivity gain is given by $G(\theta_a, \theta_d)$, where θ_a is the antenna 3-dB beamwidth for the azimuth orientation in the horizontal direction and θ_d is the antenna 3-dB beamwidth for the elevation angles in the TBS, with main-lobe gain G_M and side-lobe gain G_m . By adjusting the antenna direction toward the corresponding UE, the UE benefits from the high main-lobe gain G_M . Moreover, since we evaluate the average directivity gain in our systems, the effect of misalignment is ignored in the rest of this paper. Considering the interfering transmission, the beamforming gain and its association probability can be expressed as follows

$$G = \begin{cases} G_M, & p_M = \frac{\theta_a}{2\pi} \cdot \frac{\theta_d}{\pi} \\ G_m, & p_m = 1 - \frac{\theta_a}{2\pi} \cdot \frac{\theta_d}{\pi}, \end{cases} \quad (2)$$

where we assume that the azimuth angle ψ is uniformly distributed in the range of $[-\pi, \pi]$, and the depression angle ϕ is uniformly distributed in the range $[-\frac{\pi}{2}, \frac{\pi}{2}]$ for all interfering transmissions.

C. Channel Characteristics in the NOMA Enabled tier

In the second tier of the networks, the channel between the ABS and the UE is highly affected by the density and altitude of obstacles in the environment, then the A2G channels contain both LoS and NLoS links. In this paper, we adopt a measurement based on the probabilistic model for LoS/NLoS propagation [4], which is suitable for sub-6GHz scenarios. The probability expressions of LoS/NLoS links are defined as $P_L(x)$ and $P_N(x)$, respectively. The LoS link is shown as

$$P_L(x) = \frac{1}{1 + a \exp(-b(\frac{180}{\pi}) \tan^{-1}(\frac{h}{x} - a))}, \quad (3)$$

where a and b are referred to as the S-curve parameters which are related to the transmission environment, and x denotes the horizontal distance between the ABS and the UE. Note that a higher ABS altitude results in a higher LoS probability due to fewer obstacles. Accordingly, the NLoS link probability is given by $P_N(x) = 1 - P_L(x)$.

Since each link between the ABS and the UE is either in a LoS or NLoS condition with probability $P_L(x)$ and $P_N(x)$, the set of ABSs can be divided into two independent non-homogeneous PPPs Φ_L and Φ_N with $\Phi_A = \Phi_L \cup \Phi_N$, which denote the LoS ABSs and the NLoS ABSs, respectively. The corresponding densities of Φ_L and Φ_N with respect to the horizontal distance x from the typical UE are given by $\lambda_L(x) = 2\pi\lambda_A P_L(x)$ and $\lambda_N(x) = 2\pi\lambda_A P_N(x)$, respectively. In the following, we use $x_{L,i}$ and $x_{N,i}$ to denote the horizontal locations of the LoS and NLoS ABSs, respectively.

We consider different channel parameters for LoS/NLoS links in the A2G channels. The additive loss and path loss exponents of the LoS link in the A2G channels are denoted by C_L and α_L , and accordingly we introduce C_N and α_N in the NLoS state. Therefore, the channel gains are denoted as H_L and H_N , which follow the Gamma distribution with parameter $\Gamma(m_L, \frac{1}{m_L})$ and $\Gamma(m_N, \frac{1}{m_N})$, respectively.

D. UE Association

In this UAV-aided HetNets, a UE is allowed to access the mmWave tier or the NOMA enabled tier in order to provide the best coverage. The flexible UE association is based on the maximum

long-term averaged received power at the UE of each tier. Intuitively, the typical UE will choose to connect to the BS which has the minimum distance to the UE for both of the tiers.

1) *Average Received Power in mmWave Tier*: Denoting $R_{T,0}$ as the minimum horizontal distance between the typical UE and the TBSs. We assume that the transmit power of all the TBSs is P_T . Thus, the average received power at the UE connected to the TBS is given by

$$P_{r,T} = G_M P_T C_T R_{T,0}^{-\alpha_T} \mathbf{1}(R_B - R_{T,0}) \triangleq \eta_T R_{T,0}^{-\alpha_T} \mathbf{1}(R_B - R_{T,0}), \quad (4)$$

where G_M is the directional beamforming gain.

2) *Average Received Power in the NOMA Enabled Tier* : In the NOMA enabled tier, we adopt UE pairing to implement NOMA in order to reduce the complexity [24]. Compared with the UE association in the OMA scheme, NOMA allocates different power levels to multiple UEs by exploiting power sparsity. The locations of the UEs are also not pre-determined due to the random spatial topology of the stochastic model. As such, we always assume that a near UE is chosen as the typical one first no matter it lies in a LoS/NLoS state [25], and we denote $R_{L,0}$ and $R_{N,0}$ as the minimum distance between the typical UE and the LoS/NLoS ABSs. Then the average received power at the UE connected to the LoS/NLoS ABS can be expressed as

$$P_{r,L} = a_n P_A C_L R_{L,0}^{-\alpha_L} \triangleq \eta_L R_{L,0}^{-\alpha_L}, \quad (5)$$

and

$$P_{r,N} = a_n P_A C_N R_{N,0}^{-\alpha_N} \triangleq \eta_N R_{N,0}^{-\alpha_N}, \quad (6)$$

respectively, where P_A denotes the transmit power of all the ABSs, and a_n denotes the power allocation factor for the near UE.

E. SINR Analysis

Due to the fact that the TBS tier and ABS tier utilize distinctive carrier frequencies, the signals in these two tiers do not affect each other.

1) *mmWave Tier Transmission*: The SINR at the typical UE when it is connected to a TBS at a distance $R_{T,0}$ can be expressed as

$$\gamma_T = \frac{G_M P_T C_T R_{T,0}^{-\alpha_T} H_{T,0}}{I_T + \sigma^2}, \quad (7)$$

where $R_{T,0} \leq R_B$, and $I_T = \sum_{x_{T,i} \in \Phi_T \cap \mathcal{B}(0, R_B) \setminus x_{T,0}} G_i P_T C_T R_{T,i}^{-\alpha_T} H_{T,i}$ is the interference from the TBS tier. $H_{T,0}$ is the channel gain between the typical UE and the serving TBS, $H_{T,i}$ and

$R_{T,i}$ refer to the channel gain and the distance between typical UE and the TBS i (except for the serving BS), respectively. The value and probability of G_i can be obtained through (2). σ^2 denotes the noise power. Both $H_{T,0}$ and $H_{T,i}$ follow the distribution of $\Gamma(m_T, \frac{1}{m_T})$.

2) *NOMA Enabled Tier Transmission*: In the ABS tier, without loss of generality, we consider that each ABS is associated with one UE in the previous round of the UE association process. For simplicity, we follow the assumption in [25] where the distance between the associated UEs and the connected ABSs are the same, which are arbitrary values and denoted as $R_f \geq h$. Since the path loss is more dominant compared with the small scale fading, we apply the SIC operation at the near UE side. However, it is not pre-determined that the typical UE is the near UE or the far UE, we have the following near UE case and far UE case. We first assume that the typical UE is in a LoS state.

a) *Near UE in a LoS state case*: When the typical UE is the near UE in a LoS state, i.e., $R_{L,0} \leq R_f$, the typical UE will first decode the information of the fixed UE to the same LoS ABS with the following SINR

$$\gamma_{t \rightarrow f, near}^L = \frac{a_m P_A C_L R_{L,0}^{-\alpha_L} H_{L,0}}{a_n P_A C_L R_{L,0}^{-\alpha_L} H_{L,0} + I_L + I_N + \sigma^2}, \quad (8)$$

where a_m denotes the power allocation factor for the far UE which satisfies $a_m > a_n$ and $a_m + a_n = 1$. $I_L = \sum_{x_{L,i} \in \Phi_L \setminus x_{L,0}} P_A C_L R_{L,i}^{-\alpha_L} H_{L,i}$ denotes the interference from the LoS ABSs and $I_N = \sum_{x_{N,i} \in \Phi_N} P_A C_N R_{N,i}^{-\alpha_N} H_{N,i}$ denotes the interference from the NLoS ABSs. $H_{L,0}$ is the channel gain between the typical UE and the associated LoS ABS. $H_{L,i}$ and $R_{L,i}$ refer to the channel gain and the distance between the typical UE and LoS ABS i (except for the serving ABS), respectively. $H_{N,i}$ and $R_{N,i}$ refer to the channel gain and the distance between the typical UE and NLoS ABS i , respectively. $H_{L,0}$ and $H_{L,i}$ follow the distribution of $\Gamma(m_L, \frac{1}{m_L})$. $H_{N,i}$ follows the distribution of $\Gamma(m_N, \frac{1}{m_N})$.

If the information of the fixed UE can be decoded successfully, the typical UE will decode its own message with the following SINR

$$\gamma_{t, near}^L = \frac{a_n P_A C_L R_{L,0}^{-\alpha_L} H_{L,0}}{I_L + I_N + \sigma^2}. \quad (9)$$

For the fixed UE (far UE) served by the same ABS, the signal can be decoded by treating the message of the typical UE as interference, then the SINR for the fixed UE can be expressed as

$$\gamma_{f, near}^L = \frac{a_m P_A C_L R_f^{-\alpha_L} H_{L,f}}{a_n P_A C_L R_f^{-\alpha_L} H_{L,f} + I_L + I_N + \sigma^2}, \quad (10)$$

where $H_{L,f}$ refers to the channel gain between the fixed UE and the serving LoS ABS.

b) Far UE in a LoS state case: On the other hand, when the typical UE has a larger distance to the serving LoS ABS than the fixed UE, i.e., $R_{L,0} > R_f$, the fixed UE will first decode the information of the typical UE with the following SINR

$$\gamma_{f \rightarrow t, far}^L = \frac{a_m P_A C_L R_f^{-\alpha_L} H_{L,f}}{a_n P_A C_L R_f^{-\alpha_L} H_{L,f} + I_L + I_N + \sigma^2}. \quad (11)$$

Once the information of the typical UE can be decoded successfully, and by applying the SIC technique, the SINR to decode its own message at the fixed UE is given by

$$\gamma_{f, far}^L = \frac{a_n P_A C_L R_f^{-\alpha_L} H_{L,f}}{I_L + I_N + \sigma^2}. \quad (12)$$

For the typical UE that connects to the same LoS ABS, the SINR can be expressed as

$$\gamma_{t, far}^L = \frac{a_m P_A C_L R_{L,0}^{-\alpha_L} H_{L,0}}{a_n P_A C_L R_{L,0}^{-\alpha_L} H_{L,0} + I_L + I_N + \sigma^2}. \quad (13)$$

c) NLoS state case: When the typical UE is associated to a NLoS ABS, the typical UE can be a near UE or a far UE as well. The SINR analysis in NLoS state is similar to that of the LoS state case, and we omit the details here.

III. RELEVANT DISTANCE DISTRIBUTIONS AND ASSOCIATION ANALYSIS

In this section, we focus on providing the distribution of the distances between the typical UE and the serving TBS, NLoS ABS and LoS ABS, respectively, in the HetNets system. Furthermore, we derive the expressions for the association probabilities. At last, the distance distributions are characterized given that the typical UE is associated with a TBS, a NLoS ABS or a LoS ABS.

A. Distance Distributions of the nearest BSs

Lemma 1. *The probability density function (PDF) of $R_{L,0}$, $R_{N,0}$ and $R_{T,0}$ are given by*

$$f_{R_{L,0}}(r) = 2\pi\lambda_A r P_L(\sqrt{r^2 - h^2}) \exp\left(-2\pi\lambda_A \int_0^{\sqrt{r^2 - h^2}} x P_L(x) dx\right), \quad r \geq h \quad (14)$$

$$f_{R_{N,0}}(r) = 2\pi\lambda_A r P_N(\sqrt{r^2 - h^2}) \exp\left(-2\pi\lambda_A \int_0^{\sqrt{r^2 - h^2}} x P_N(x) dx\right), \quad r \geq h \quad (15)$$

$$f_{R_{T,0}}(r) = \begin{cases} 2\pi\lambda_T r \exp(-\pi\lambda_T r^2), & r \leq R_B \\ 0, & r > R_B \end{cases} \quad (16)$$

Proof. Using a similar method to Lemma 1 of [13], the above expressions can be obtained.

B. Distance of the nearest interfering BSs

Due to the deployment of mmWave and the special channel characteristics of A2G channels, the distance of the nearest interfering BSs is not easy to observe. The following remarks show clear insights on the locations of the nearest interfering BSs, which will be useful to derive the main results of this paper.

1) *The typical UE is associated with a NLoS ABS:* When the typical UE is associated with a NLoS ABS, we have the following lemma and assumption, which help us to derive the minimum distance of the interfering LoS ABS.

Lemma 2. *The probability that the typical UE has at least one TBS in $\mathcal{B}(0, R_B)$ can be calculated by $Q_T \triangleq F_{R_{T,0}}(R_B) = 1 - \exp(-\pi\lambda_T R_B^2)$.*

Assumption 1. *When there exists a TBS in $\mathcal{B}(0, R_B)$, the typical UE never associates with a NLoS ABS.*

If there exists a TBS in $\mathcal{B}(0, R_B)$, and the typical UE is associated with a NLoS ABS. Then the average received power at a height h connecting to a NLoS ABS should not be smaller than the average received power at a distance R_B connecting to a TBS, resulting in the condition $h \leq (\frac{\eta_N}{\eta_T})^{\frac{1}{\alpha_N}} R_B^{\frac{\alpha_T}{\alpha_N}}$ satisfied. With a huge path loss and additive loss in NLoS channels, this condition is not satisfied normally.

Remark 1. *Given that the typical UE is associated with a NLoS ABS at a distance r , the minimum distance of the interfering LoS ABS $\tau_{L|N}(r)$ is given by*

$$\tau_{L|N}(r) = \left(\frac{\eta_L}{\eta_N}\right)^{\frac{1}{\alpha_L}} r^{\frac{\alpha_N}{\alpha_L}}, \quad r \geq h \quad (17)$$

Proof. According to (5) and (6), the average received power of the UE associated with a NLoS ABS at a distance r is given by $\eta_N r^{-\alpha_N}$. The minimum distance of the interfering LoS ABS $\tau_{L|N}(r)$ can be obtained by solving $\eta_N r^{-\alpha_N} = \eta_L \tau_{L|N}^{-\alpha_L}(r)$.

2) *The typical UE is associated with a LoS ABS:* When the typical UE is associated with a LoS ABS at a distance r , depending on whether there exists a TBS in $\mathcal{B}(0, R_B)$, we have two cases. We first denote $l_{L,h} \triangleq (\frac{\eta_L}{\eta_N})^{\frac{1}{\alpha_L}} h^{\frac{\alpha_N}{\alpha_L}}$, which is the distance between the typical UE and a LoS ABS when its average received power is the same as that the average received power from a NLoS ABS at a distance of h , i.e., $\tau_{L|N}(h)$. We then denote $l_{L,T} \triangleq (\frac{\eta_L}{\eta_T})^{\frac{1}{\alpha_L}} R_B^{\frac{\alpha_T}{\alpha_L}}$ as the

maximum association distance between the typical UE and a LoS ABS when there exists a TBS in $\mathcal{B}(0, R_B)$. As such, if there exists a TBS in $\mathcal{B}(0, R_B)$, then only the LoS ABSs which lie in the range of $h \leq r \leq l_{L,T}$ can be associated to the typical UE.

Remark 2. Given that the typical UE is associated with a LoS ABS at a distance r , the minimum distances of the interfering TBS $\tau_{T|L}(r)$ and NLoS ABS $\tau_{N|L}(r)$ are given by

$$\tau_{T|L}(r) = \left(\frac{\eta_T}{\eta_L} \right)^{\frac{1}{\alpha_T}} r^{\frac{\alpha_L}{\alpha_T}}, \quad h \leq r \leq l_{L,T}. \quad (18)$$

If there exists a TBS in $\mathcal{B}(0, R_B)$, and $l_{L,T} \geq l_{L,h}$ is satisfied, we have

$$\tau_{N|L}(r) = \begin{cases} h, & h \leq r \leq l_{L,h} \\ \left(\frac{\eta_N}{\eta_L} \right)^{\frac{1}{\alpha_N}} r^{\frac{\alpha_L}{\alpha_N}}, & l_{L,h} < r \leq l_{L,T}. \end{cases} \quad (19)$$

Otherwise when $l_{L,h} > l_{L,T}$, we have

$$\tau_{N|L}(r) = h, \quad h \leq r \leq l_{L,T}. \quad (20)$$

If there does not exist a TBS in $\mathcal{B}(0, R_B)$, $\tau_{N|L}(r)$ can be expressed as

$$\tau_{N|L}(r) = \begin{cases} h, & h \leq r < l_{L,h} \\ \left(\frac{\eta_N}{\eta_L} \right)^{\frac{1}{\alpha_N}} r^{\frac{\alpha_L}{\alpha_N}}, & r \geq l_{L,h} \end{cases} \quad (21)$$

Proof. The proof is similar to the proof in Remark 1, therefore it is omitted here.

3) *The typical UE is associated with a TBS:* When the typical UE is associated with a TBS, the condition $0 \leq r \leq R_B$ should be satisfied. We first denote $l_{T,L} \triangleq \left(\frac{\eta_T}{\eta_L} \right)^{\frac{1}{\alpha_T}} h^{\frac{\alpha_L}{\alpha_T}}$ as the distance between a UE and a TBS when its average received power is the same as the average received power of a LoS ABS at a distance of h , and similarly we denote $l_{T,N} \triangleq \left(\frac{\eta_T}{\eta_N} \right)^{\frac{1}{\alpha_T}} h^{\frac{\alpha_N}{\alpha_T}}$.

Remark 3. Given that the typical UE is associated with a TBS at a distance r , the minimum distances of the interfering LoS ABS $\tau_{L|T}(r)$ and NLoS ABS $\tau_{N|T}(r)$ are shown below

Condition	$\tau_{L T}(r)$	$\tau_{N T}(r)$
$R_B \leq l_{T,L} \leq l_{T,N}$	$h, \quad 0 \leq r \leq R_B$	$h, \quad 0 \leq r \leq R_B$
$l_{T,L} \leq R_B \leq l_{T,N}$	$h, \quad 0 \leq r < l_{T,L}$ $\left(\frac{\eta_L}{\eta_T} \right)^{\frac{1}{\alpha_L}} r^{\frac{\alpha_T}{\alpha_L}}, \quad l_{T,L} \leq r \leq R_B$	$h, \quad 0 \leq r \leq R_B$
$R_B \geq l_{T,N} \geq l_{T,L}$	$h, \quad 0 \leq r < l_{T,L}$ $\left(\frac{\eta_L}{\eta_T} \right)^{\frac{1}{\alpha_L}} r^{\frac{\alpha_T}{\alpha_L}}, \quad l_{T,L} \leq r \leq R_B$	$h, \quad 0 \leq r < l_{T,N}$ $\left(\frac{\eta_N}{\eta_T} \right)^{\frac{1}{\alpha_N}} r^{\frac{\alpha_T}{\alpha_N}}, \quad l_{T,N} \leq r \leq R_B$

Proof. The proof is similar to the proof in **Remark 1** and **Remark 2**, therefore it is omitted here.

C. Association Probability

We first study the probability that typical UE is associated with a NLoS ABS.

Lemma 3. *The probability that a typical UE connects to a NLoS ABS can be calculated as*

$$A_N = (1 - Q_T) \int_h^\infty \exp\left(-2\pi\lambda_A \int_0^{\sqrt{\tau_{L|N}^2(r)-h^2}} x P_L(x) dx\right) f_{R_{N,0}}(r) dr. \quad (22)$$

Proof. Using a similar method to Lemma 2 of [13], and considering there does not exist a TBS in $\mathcal{B}(0, R_B)$, the above expressions can be obtained.

We then study the probability that the typical UE is associated with a LoS ABS.

Lemma 4. *The probability that the typical UE has at least one LoS ABS when $h \leq R_{L,0} \leq l_{L,T}$ can be calculated by $Q_L \triangleq F_{R_{L,0}}(l_{L,T}) = 1 - \exp\left(-2\pi\lambda_A \int_0^{\sqrt{l_{L,T}^2-h^2}} x P_L(x) dx\right)$.*

Lemma 5. *The probability that a typical UE connects to a LoS ABS can be calculated as*

$$A_L = A_{L,1} + A_{L,2}, \quad (23)$$

where $A_{L,1}$ and $A_{L,2}$ are the association probability related to the cases when there does not exist a TBS and there exists a TBS in $\mathcal{B}(0, R_B)$, respectively. $A_{L,1}$ and $A_{L,2}$ are given by

$$A_{L,1} = (1 - Q_T) \left[\int_h^{l_{L,h}} f_{R_{L,0}}(r) dr + \int_{l_{L,h}}^\infty \exp\left(-2\pi\lambda_A \int_0^{\sqrt{\tau_{N|L}^2(r)-h^2}} x P_N(x) dx\right) f_{R_{L,0}}(r) dr \right], \quad (24)$$

and

$$A_{L,2} = Q_T Q_L \mathbb{P}(A_{L,2}^N) \mathbb{P}(A_{L,2}^T), \quad (25)$$

respectively, where $\mathbb{P}(A_{L,2}^N) = 1$, if $l_{L,h} > l_{L,T}$, or

$$\mathbb{P}(A_{L,2}^N) = \frac{\int_h^{l_{L,h}} f_{R_{L,0}}(r) dr + \int_{l_{L,h}}^{l_{L,T}} \exp\left(-2\pi\lambda_A \int_0^{\sqrt{\tau_{N|L}^2(r)-h^2}} x P_N(x) dx\right) f_{R_{L,0}}(r) dr}{Q_L}, \quad (26)$$

and

$$\mathbb{P}(A_{L,2}^T) = \frac{\int_h^{l_{L,T}} \left[\exp\left(-\pi\lambda_T \tau_{T|L}^2(r)\right) - (1 - Q_T) \right] f_{R_{L,0}}(r) dr}{Q_L Q_T}. \quad (27)$$

Proof. See Appendix A.

Finally, we study the probability that the typical UE is associated with a TBS.

Proposition 1. *The probability that a typical UE connects to a TBS can be calculated as*

$$A_T = 1 - A_N - A_L. \quad (28)$$

D. Conditional distance distribution of the serving BS

Now, denoting $\hat{R}_{N,0}$, $\hat{R}_{L,0}$ and $\hat{R}_{T,0}$ as the minimum distance between the typical UE and the serving BS given that it is associated with the NLoS ABS, LoS ABS and TBS, respectively. The following lemmas characterize the distributions of $\hat{R}_{N,0}$, $\hat{R}_{L,0}$ and $\hat{R}_{T,0}$.

Lemma 6. *The probability density function (PDF) of $\hat{R}_{N,0}$ is given by*

$$f_{\hat{R}_{N,0}}(r) = \frac{f_{R_{N,0}}(r)}{A_N} \exp\left(-2\pi\lambda_A \int_0^{\sqrt{\tau_{L|N}^2(r)-h^2}} x P_L(x) dx\right) (1 - Q_T). \quad (29)$$

Proof. Denoting B_N as the event that the typical UE is associated with a NLoS ABS. Then we have

$$f_{\hat{R}_{N,0}}(r) = \frac{d}{dr} \mathbb{P}(\hat{R}_{N,0} \leq r) = \frac{d}{dr} \mathbb{P}(R_{N,0} \leq r | B_N) = \frac{d}{dr} \frac{\mathbb{P}(R_{N,0} \leq r \cap B_N)}{A_N}, \quad (30)$$

where $\mathbb{P}(R_{N,0} \leq r \cap B_N)$ can be derived as

$$\begin{aligned} \mathbb{P}(R_{N,0} \leq r \cap B_N) &= \mathbb{P}\left(X_{L,0} > \sqrt{\tau_{L|N}^2(R_{N,0}) - h^2} \cap R_{N,0} \leq r\right) (1 - Q_T) \\ &= \int_h^r \exp\left(-2\pi\lambda_A \int_0^{\sqrt{\tau_{L|N}^2(\tilde{r})-h^2}} x P_L(x) dx\right) f_{R_{N,0}}(\tilde{r}) d\tilde{r} (1 - Q_T). \end{aligned} \quad (31)$$

Then taking the first order derivative, we can obtain the expressions in (29).

Given that the typical UE is associated with a LoS ABS, depending on whether there exists a TBS in $\mathcal{B}(0, R_B)$, and utilizing the results in **Remark 2**, we have the following lemma.

Lemma 7. *The PDF of $\hat{R}_{L,0}$ is given by $f_{\hat{R}_{L,0,1}}(r)$ or $f_{\hat{R}_{L,0,2}}(r)$, where $f_{\hat{R}_{L,0,1}}(r)$ is the PDF of $\hat{R}_{L,0}$ when there does not exist a TBS in $\mathcal{B}(0, R_B)$, and $f_{\hat{R}_{L,0,2}}(r)$ is the PDF of $\hat{R}_{L,0}$ when there exists a TBS in $\mathcal{B}(0, R_B)$. $f_{\hat{R}_{L,0,1}}(r)$ and $f_{\hat{R}_{L,0,2}}(r)$ are given by*

$$f_{\hat{R}_{L,0,1}}(r) = \begin{cases} \frac{f_{R_{L,0}}(r)}{A_L} (1 - Q_T), & h \leq r \leq l_{L,h} \\ \frac{f_{R_{L,0}}(r)}{A_L} \exp\left(-2\pi\lambda_A \int_0^{\sqrt{\tau_{N|L}^2(r)-h^2}} x P_N(x) dx\right) (1 - Q_T), & r > l_{L,h}. \end{cases} \quad (32)$$

When the condition $l_{L,h} > l_{L,T}$ is satisfied,

$$f_{\hat{R}_{L,0,2}}(r) = \frac{f_{R_{L,0}}(r)}{A_L} \left[\exp(-\pi\lambda_T\tau_T^2|L(r)) - (1 - Q_T) \right], \quad h \leq r \leq l_{L,T}. \quad (33)$$

When the condition $l_{L,T} \geq l_{L,h}$ is satisfied,

$$f_{\hat{R}_{L,0,2}}(r) = \begin{cases} \frac{f_{R_{L,0}}(r)}{A_L} \left[\exp(-\pi\lambda_T\tau_T^2|L(r)) - (1 - Q_T) \right], & h \leq r \leq l_{L,h} \\ \frac{f_{R_{L,0}}(r)}{A_L} \left[\exp(-\pi\lambda_T\tau_T^2|L(r)) - (1 - Q_T) \right] \exp\left(-2\pi\lambda_A \int_0^{\sqrt{\tau_{N|L}^2(r)-h^2}} x P_N(x) dx\right), & l_{L,h} < r \leq l_{L,T}. \end{cases} \quad (34)$$

Proof. The proof is similar to that in **Lemma 6**, therefore it is omitted here.

Given that the typical UE is associated with a TBS, and we consider a typical condition when $l_{T,L} \leq R_B \leq l_{T,N}$. Utilizing the results in **Remark 3**, we have the following lemma.

Lemma 8. When the condition $l_{T,L} \leq R_B \leq l_{T,N}$ is satisfied, the PDF of $\hat{R}_{T,0}$ is given by

$$f_{\hat{R}_{T,0}}(r) = \begin{cases} \frac{f_{R_{T,0}}(r)}{A_T}, & 0 \leq r \leq l_{T,L} \\ \frac{f_{R_{T,0}}(r)}{A_T} \exp\left(-2\pi\lambda_A \int_0^{\sqrt{\tau_{L|T}^2(r)-h^2}} x P_L(x) dx\right), & l_{T,L} < r \leq R_B \end{cases} \quad (35)$$

Proof. The proof is similar to that in **Lemma 6** and **Lemma 7**, therefore it is omitted here.

IV. COVERAGE PROBABILITY ANALYSIS

The coverage probability is defined as that a typical UE can successfully transmit signals with a targeted SINR. To begin with, we derive the Laplace transform of the interference.

A. Laplace Transform of Interference

Since the ABSs and the TBSs utilize different frequencies, the inter-tier interference can be avoided. We first consider the case that the interference signals are from the TBSs.

Lemma 9. The Laplace transform of interference from TBSs to a typical UE is given by

$$L_{I_T}(s) = \exp\left[\frac{-2\pi\lambda_T}{\alpha_T} \sum_{j \in \{M,m\}} \sum_{i=1}^{m_T} p_j \binom{m_T}{i} \left(\frac{sP_T C_T G_j}{m_T}\right)^{\frac{2}{\alpha_T}} (-1)^{\frac{2}{\alpha_T}-i+1} \times \left(B\left(t_{j,u}; i - \frac{2}{\alpha_T}, 1 - m_T\right) - B\left(t_{j,l}; i - \frac{2}{\alpha_T}, 1 - m_T\right) \right)\right], \quad (36)$$

where $t_{j,l} = -\frac{sP_T C_T G_j}{m_T R_{T,0}^{\alpha_T}}$, $t_{j,u} = -\frac{sP_T C_T G_j}{m_T R_B^{\alpha_T}}$, and $B(\cdot; \cdot, \cdot)$ is the incomplete Beta function.

Proof. See Appendix B.

Then we consider the scenario where the interference signals are from ABSs.

Lemma 10. *The Laplace transform of interference from ABSs to a typical UE is given by*

$$L_{I_A}(s) = \exp \left(-2\pi\lambda_A \int_{w_{L,l}(r)}^{w_{L,u}(r)} \left(1 - \left(1 + \frac{sP_A C_L}{m_L(x^2 + h^2)^{\frac{\alpha_L}{2}}} \right)^{-m_L} \right) P_L(x) dx \right) \\ \times \exp \left(-2\pi\lambda_A \int_{w_{N,l}(r)}^{w_{N,u}(r)} \left(1 - \left(1 + \frac{sP_A C_N}{m_N(x^2 + h^2)^{\frac{\alpha_N}{2}}} \right)^{-m_N} \right) P_N(x) dx \right), \quad (37)$$

where $w_{L,l}(r)$, $w_{L,u}(r)$, $w_{N,l}(r)$, and $w_{N,u}(r)$ are given as follows.

Condition	$w_{L,l}(r)$	$w_{L,u}(r)$	$w_{N,l}(r)$	$w_{N,u}(r)$
B_N	$\sqrt{\tau_{L N}^2(r) - h^2}$	∞	$\sqrt{r^2 - h^2}$	∞
B_L	$\sqrt{r^2 - h^2}$	∞	$\sqrt{\tau_{N L}^2(r) - h^2}$	∞

Proof. The interference from ABSs I_A contains both the interference from LoS ABSs I_L and interference from NLoS ABSs I_N , then the Laplace transform of I_A equals to $L_{I_A}(s) = L_{I_L}(s)L_{I_N}(s)$. Following the same steps in **Lemma 9**, we can obtain the above expressions.

B. Coverage Probability in mmWave Tier

Given that the typical UE is associated with a TBS, the coverage probability is defined as

$$P_T^C = \mathbb{P} \left(\frac{G_M P_T C_T R_{T,0}^{-\alpha_T} H_{T,0}}{I_T + \sigma^2} \geq \nu_T \right), \quad (38)$$

where ν_T is the targeted SINR of the typical UE.

Lemma 11. *The exact and approximated expression of P_T^C can be expressed as*

$$P_T^C = \int_0^{R_B} \left(\sum_{k=0}^{m_T-1} \sum_{p=0}^k \binom{k}{p} \frac{r^{\alpha_T k} (m_T \varepsilon_T)^k}{k!} \exp(-m_T r^{\alpha_T} \varepsilon_T \sigma^2) (\sigma^2)^p \times \left[(-1)^{k-p} \frac{\partial^{k-p}}{\partial s^{k-p}} L_{I_T}(s) \right] \right) f_{\hat{R}_{T,0}}(r) dr \\ \approx \int_0^{R_B} \left(\sum_{k=1}^{m_T} (-1)^{k+1} \binom{m_T}{k} e^{-kb_T r^{\alpha_T} \varepsilon_T \sigma^2} L_{I_T}(kb_T r^{\alpha_T} \varepsilon_T) \right) f_{\hat{R}_{T,0}}(r) dr. \quad (39)$$

where $\varepsilon_T \triangleq \frac{\nu_T}{G_M P_T C_T}$, and $s = m_T \varepsilon_T r^{\alpha_T}$.

Proof. See Appendix C.

It is challenging to obtain exact closed-form expressions for P_T^C . Accordingly, we adopt the Gaussian-Chebyshev quadrature [26] to find an approximation of (39) as follows:

Corollary 1. *When the condition $l_{T,L} \leq R_B \leq l_{T,N}$ is satisfied, (39) can be approximated by*

$$P_T^C \approx \frac{1}{2A_T} \sum_{i=1}^N \sum_{k=1}^{m_T} \omega_N (-1)^{k+1} \binom{m_T}{k} \sqrt{1 - r_i^2} \left\{ l_{T,L} e^{-\xi_k c_i^{\alpha_T} \sigma^2} L_{I_T}(\xi_k c_i^{\alpha_T}) f_{R_{T,0}}(c_i) + \right. \\ \left. (R_B - l_{T,L}) e^{-\xi_k d_i^{\alpha_T} \sigma^2} L_{I_T}(\xi_k d_i^{\alpha_T}) f_{R_{T,0}}(d_i) \exp \left(-2\pi\lambda_A \int_0^{\sqrt{\tau_{L|T}^2(d_i) - h^2}} x P_L(x) dx \right) \right\}, \quad (40)$$

where $\xi_k = kb_T \varepsilon_T$, and N is a parameter to ensure a complexity-accuracy tradeoff, $\omega_N = \frac{\pi}{N}$, $r_i = \cos\left(\frac{2i-1}{2n}\pi\right)$, $c_i = \frac{l_{T,L}}{2}r_i + \frac{l_{T,L}}{2}$, and $d_i = \frac{R_B - l_{T,L}}{2}r_i + \frac{R_B - l_{T,L}}{2}$.

C. Coverage Probability in the NOMA Enabled Tier

According to the NOMA decoding strategy, two cases will be considered, i.e. the near UE case and the far UE case. We first consider that the typical UE is in the LoS state.

1) *LoS Near UE Case:* In this case, i.e., $R_{L,0} \leq R_f$, when the following conditions hold, successful decoding will occur:

- The typical UE can decode the information of the fixed UE served by the same BS.
- After the SIC process, the typical UE can decode its own information.

Thus, the coverage probability in this case can be expressed as

$$P_{cov,near|LoS}(R_{L,0}) = \mathbb{P}(\gamma_{t \rightarrow f,near}^L > \epsilon_f, \gamma_{t,near}^L > \epsilon_t), \quad (41)$$

where ϵ_f and ϵ_t are the targeted SINR of the fixed UE and the typical UE, respectively.

Based on (41), the coverage probability of a typical UE for the near UE case in a LoS state is given in the following Proposition.

Proposition 2. *If $a_m - a_n \epsilon_f \geq 0$ holds, the exact and approximated coverage probability of a typical UE for the LoS UE case can be expressed as*

$$\begin{aligned} & P_{cov,near|LoS}(R_{L,0}) \\ &= \sum_{k=0}^{m_L-1} \sum_{p=0}^k \binom{k}{p} \frac{R_{L,0}^{\alpha L k} (m_L \epsilon^*)^k}{k! (P_A C_L)^k} \exp\left(-m_L \frac{\epsilon^* R_{L,0}^{\alpha L}}{P_A C_L} \sigma^2\right) (\sigma^2)^p \mathbb{E}_{I_A} \left[\exp\left(-m_L \frac{\epsilon^* R_{L,0}^{\alpha L}}{P_A C_L} I_A\right) (I_A)^{k-p} \right] \\ &\approx \sum_{k=1}^{m_L} (-1)^{k+1} \binom{m_L}{k} e^{-kb_L \frac{\epsilon^* R_{L,0}^{\alpha L} \sigma^2}{P_A C_L}} L_{I_A} \left(kb_L \frac{\epsilon^* R_{L,0}^{\alpha L}}{P_A C_L} \right), \end{aligned} \quad (42)$$

where $\epsilon^* = \max\left\{\frac{\epsilon_f}{a_m - a_n \epsilon_f}, \frac{\epsilon_t}{a_n}\right\}$ and $b_L = m_L (m_L!)^{-\frac{1}{m_L}}$. Otherwise $P_{cov,near|LoS}(R_{L,0}) = 0$.

Proof. Substituting (8) and (9) into (41), and following the same steps in **Appendix C**, we can obtain the exact expression of $P_{cov,near|LoS}(R_{L,0})$. Similarly, by adopting the Alzer's Lemma [29], we obtain the results in (42).

2) *LoS Far UE Case:* For this case, i.e., $R_{L,0} > R_f$, successful decoding will occur if the typical UE can decode its own information by treating the fixed UE as noise. The coverage probability of a typical UE for the far UE case in a LoS state is given in the following proposition.

Proposition 3. If $a_m - a_n \epsilon_t \geq 0$ holds, the coverage probability of a typical UE for the LoS UE case can be expressed as

$$P_{cov, far|LoS}(R_{L,0}) \approx \sum_{k=1}^{m_L} (-1)^{k+1} \binom{m_L}{k} e^{-kb_L \frac{\epsilon_t^f R_{L,0}^{\alpha_L} \sigma^2}{P_{AC_L}}} L_{IA} \left(kb_L \frac{\epsilon_t^f R_{L,0}^{\alpha_L}}{P_{AC_L}} \right), \quad (43)$$

otherwise $P_{cov, far|LoS}(R_{L,0}) = 0$, where $\epsilon_t^f = \frac{\epsilon_t}{a_m - a_n \epsilon_t}$.

Proof. By following the similar procedure, with interchanging ϵ^* with ϵ_t^f , we obtain the desired results.

Remark 4. *Proposition 2 and Proposition 3 provide the basic power allocation guidelines for the NOMA enabled ABSs networks. The targeted SINR threshold of the typical UE and the fixed UE both determine the coverage probability of a typical UE when it is associated with an ABS. Furthermore, inappropriate power allocation such as $a_m - a_n \epsilon_f < 0$ and $a_m - a_n \epsilon_t < 0$ cause the coverage probability in the NOMA enabled tier always being zero.*

Theorem 1. The coverage probability of a typical UE associated with a LoS ABS is given by

$$P_{cov, LoS}(\epsilon_f, \epsilon_t) = \sum_{i=1}^2 \left[\int_h^{R_f} P_{cov, near|LoS}(r) f_{\hat{R}_{L,0,i}}(r) dr + \int_{R_f}^{\infty} P_{cov, far|LoS}(r) f_{\hat{R}_{L,0,i}}(r) dr \right]. \quad (44)$$

Proof. Based on (42) and (43), and by considering the distance distribution of a typical UE associated with a LoS ABS, the result in (44) can be easily obtained.

3) *NLoS Case:* Then we consider the case that the typical UE is associated with a NLoS ABS. By following the proof in **Proposition 2**, we can obtain

$$P_{cov, near|NLoS}(R_{N,0}) \approx \sum_{k=1}^{m_N} (-1)^{k+1} \binom{m_N}{k} e^{-kb_N \frac{\epsilon^* R_{N,0}^{\alpha_N} \sigma^2}{P_{AC_N}}} L_{IA} \left(kb_N \frac{\epsilon^* R_{N,0}^{\alpha_N}}{P_{AC_N}} \right), \quad (45)$$

where $b_N = m_N (m_N!)^{-\frac{1}{m_N}}$, and

$$P_{cov, far|NLoS}(R_{N,0}) \approx \sum_{k=1}^{m_N} (-1)^{k+1} \binom{m_N}{k} e^{-kb_N \frac{\epsilon_t^f R_{N,0}^{\alpha_N} \sigma^2}{P_{AC_N}}} L_{IA} \left(kb_N \frac{\epsilon_t^f R_{N,0}^{\alpha_N}}{P_{AC_N}} \right). \quad (46)$$

Theorem 2. The coverage probability of a typical UE associated with a NLoS ABS is given by

$$P_{cov, NLoS}(\epsilon_f, \epsilon_t) = \int_h^{R_f} P_{cov, near|NLoS}(r) f_{\hat{R}_{N,0}}(r) dr + \int_{R_f}^{\infty} P_{cov, far|NLoS}(r) f_{\hat{R}_{N,0}}(r) dr. \quad (47)$$

Proof. The proof is similar to the proof in **Theorem 1**.

Theorem 3. *The coverage probability of a typical UE associated to the NOMA enabled ABS tier is given by*

$$P_A^C(\epsilon_f, \epsilon_t) = \frac{A_L}{A_A} P_{cov,LoS}(\epsilon_f, \epsilon_t) + \frac{A_N}{A_A} P_{cov,LoS} P_{cov,NLoS}(\epsilon_f, \epsilon_t). \quad (48)$$

Proof. Based on (44) and (47), by considering that the typical UE is associated with an ABS, the result in (48) can be obtained.

V. SPECTRUM EFFICIENCY

In this section, we evaluate the spectrum efficiency of the proposed HetNets.

A. Ergodic Rate of mmWave Tier

Theorem 4. *The achievable ergodic rate of the mmWave tier can be expressed as follows*

$$R_T = \frac{1}{\ln 2} \int_0^\infty \frac{\bar{F}_{\gamma_T}(z)}{1+z} dz, \quad (49)$$

where $\bar{F}_{\gamma_T}(z)$ is approximated by

$$\bar{F}_{\gamma_T}(z) \approx \int_0^{R_B} \left(\sum_{k=1}^{m_T} (-1)^{k+1} \binom{m_T}{k} e^{-kb_T \frac{zr^{\alpha_T} \sigma^2}{G_M P_T C_T}} L_{I_T} \left(kb_T \frac{zr^{\alpha_T}}{G_M P_T C_T} \right) \right) f_{\hat{R}_{T,0}}(r) dr. \quad (50)$$

Proof. For the UE connected to a TBS, the achievable ergodic rate can be expressed as

$$\begin{aligned} R_T &= \mathbb{E}[\log_2(1 + \gamma_T)] \\ &= \int_0^\infty \mathbb{P}(\gamma_T > z) d \log_2(1 + z) = \frac{1}{\ln 2} \int_0^\infty \frac{\bar{F}_{\gamma_T}(z)}{1+z} dz. \end{aligned} \quad (51)$$

Then, given the typical UE is associated with a TBS, and following the same procedure in

Appendix C, the expression for $\bar{F}_{\gamma_T}(z)$ is given by

$$\begin{aligned} \bar{F}_{\gamma_T}(z) &= \mathbb{P} \left(\frac{G_M P_T C_T R_{T,0}^{-\alpha_T} H_{T,0}}{I_T + \sigma^2} > z \right) \\ &\approx \int_0^{R_B} \left(\sum_{k=1}^{m_T} (-1)^{k+1} \binom{m_T}{k} e^{-kb_T \frac{zr^{\alpha_T} \sigma^2}{G_M P_T C_T}} L_{I_T} \left(kb_T \frac{zr^{\alpha_T}}{G_M P_T C_T} \right) \right) f_{\hat{R}_{T,0}}(r) dr. \end{aligned} \quad (52)$$

B. Ergodic Rate of the NOMA Enabled Tier

Different from the derivations of ergodic rate in mmWave tier, the achievable ergodic rate for the NOMA enabled tier is determined by the channel conditions of UEs. If the far UE can decode its own message, the near UE can decode the message of the far UE since it has a better channel condition. The following theorems show the ergodic rate of the NOMA enabled tier.

Theorem 5. *When the typical UE is associated with an ABS, and for the LoS near UE case, the achievable ergodic rate can be expressed as*

$$R_{near|LoS} = \frac{1}{\ln 2} \int_0^\infty \frac{\bar{F}_{\gamma_{t,near}^L}(z)}{1+z} dz + \frac{1}{\ln 2} \int_0^{\frac{am}{an}} \frac{\bar{F}_{\gamma_{f,near}^L}(z)}{1+z} dz, \quad (53)$$

where

$$\bar{F}_{\gamma_{t,near}^L} \approx \sum_{i=1}^2 \int_h^{R_f} \left[\sum_{k=1}^{m_L} (-1)^{k+1} \binom{m_L}{k} e^{-kb_L \frac{zr^{\alpha_L} \sigma^2}{an P_A C_L}} L_{IA} \left(kb_L \frac{zr^{\alpha_L}}{an P_A C_L} \right) \right] f_{\hat{R}_{L,0,i}}(r) dr, \quad (54)$$

and

$$\bar{F}_{\gamma_{f,near}^L} \approx \sum_{i=1}^2 \int_h^{R_f} \left[\sum_{k=1}^{m_L} (-1)^{k+1} \binom{m_L}{k} e^{-\frac{z}{am-anz} \frac{kb_L R_f^{\alpha_L} \sigma^2}{P_A C_L}} L_{IA} \left(\frac{z}{am-anz} \frac{kb_L R_f^{\alpha_L}}{P_A C_L} \right) \right] f_{\hat{R}_{L,0,i}}(r) dr. \quad (55)$$

Proof. When the typical UE is associated with an ABS, and for the LoS near UE case, the achievable ergodic rate can be expressed as

$$\begin{aligned} R_{near|LoS} &= \mathbb{E} \left[\log_2(1 + \gamma_{t,near}^L) + \log_2(1 + \gamma_{f,near}^L) \right] \\ &= \frac{1}{\ln 2} \int_0^\infty \frac{\bar{F}_{\gamma_{t,near}^L}(z)}{1+z} dz + \frac{1}{\ln 2} \int_0^\infty \frac{\bar{F}_{\gamma_{f,near}^L}(z)}{1+z} dz. \end{aligned} \quad (56)$$

Based on (9), we can obtain the expressions for $\bar{F}_{\gamma_{t,near}^L}$ as follows

$$\begin{aligned} \bar{F}_{\gamma_{t,near}^L} &= \mathbb{P} \left(\frac{P_A C_L R_{L,0}^{-\alpha_L} H_{L,0}}{I_L + I_N + \sigma^2} > \frac{z}{a_n} \right) \\ &\approx \mathbb{E}_{R_{L,0}} \left[\sum_{k=1}^{m_L} (-1)^{k+1} \binom{m_L}{k} e^{-kb_L \frac{z R_{L,0}^{\alpha_L} \sigma^2}{an P_A C_L}} L_{IA} \left(kb_L \frac{z R_{L,0}^{\alpha_L}}{an P_A C_L} \right) \right]. \end{aligned} \quad (57)$$

Then according to whether there exists a TBS in $\mathcal{B}(0, R_B)$, we can obtain the above expressions.

Similarly, based on (10), we can obtain the expressions for $\bar{F}_{\gamma_{f,near}^L}$ as follows

$$\begin{aligned} \bar{F}_{\gamma_{f,near}^L} &= \mathbb{P} \left(H_{L,f} > \frac{z}{a_m - a_n z} \frac{R_f^{\alpha_L} (I_A + \sigma^2)}{P_A C_L} \right) \\ &\approx \mathbb{E}_{R_{L,0}} \left[\sum_{k=1}^{m_L} (-1)^{k+1} \binom{m_L}{k} e^{-\frac{z}{am-anz} \frac{kb_L R_f^{\alpha_L} \sigma^2}{P_A C_L}} L_{IA} \left(\frac{z}{am-anz} \frac{kb_L R_f^{\alpha_L}}{P_A C_L} \right) \right]. \end{aligned} \quad (58)$$

Note that for the case $z \geq \frac{am}{an}$, it is easy to observe that $\bar{F}_{\gamma_{f,near}^L} = 0$.

By following the same procedures, we can obtain the theorems below.

Theorem 6. *When the typical UE is associated with an ABS, and for the LoS far UE case, the achievable ergodic rate can be expressed as*

$$R_{far|LoS} = \frac{1}{\ln 2} \int_0^\infty \frac{\bar{F}_{\gamma_{f,far}^L}(z)}{1+z} dz + \frac{1}{\ln 2} \int_0^{\frac{am}{an}} \frac{\bar{F}_{\gamma_{t,far}^L}(z)}{1+z} dz, \quad (59)$$

where

$$\bar{F}_{\gamma_{t, far}^L} \approx \sum_{i=1}^2 \int_{R_f}^{\infty} \left[\sum_{k=1}^{m_L} (-1)^{k+1} \binom{m_L}{k} e^{-\frac{z}{a_m - a_n z} \frac{kb_f r^{\alpha_L} \sigma^2}{P_A C_L}} L_{IA} \left(\frac{z}{a_m - a_n z} \frac{kb_L r^{\alpha_L}}{P_A C_L} \right) \right] f_{\hat{R}_{L,0,i}}(r) dr, \quad (60)$$

and

$$\bar{F}_{\gamma_{f, far}^L} \approx \sum_{i=1}^2 \int_{R_f}^{\infty} \left[\sum_{k=1}^{m_L} (-1)^{k+1} \binom{m_L}{k} e^{-kb_L \frac{z R_f^{\alpha_L} \sigma^2}{a_n P_A C_L}} L_{IA} \left(kb_L \frac{z R_f^{\alpha_L}}{a_n P_A C_L} \right) \right] f_{\hat{R}_{L,0,i}}(r) dr. \quad (61)$$

Theorem 7. When the typical UE is associated with an ABS, and for the NLoS near UE case, the achievable ergodic rate can be expressed as

$$R_{near|NLoS} = \frac{1}{\ln 2} \int_0^{\infty} \frac{\bar{F}_{\gamma_{t, near}^N}(z)}{1+z} dz + \frac{1}{\ln 2} \int_0^{\frac{a_m}{a_n}} \frac{\bar{F}_{\gamma_{f, near}^N}(z)}{1+z} dz, \quad (62)$$

where

$$\bar{F}_{\gamma_{t, near}^N} \approx \int_h^{R_f} \left[\sum_{k=1}^{m_N} (-1)^{k+1} \binom{m_N}{k} e^{-kb_N \frac{z r^{\alpha_N} \sigma^2}{a_n P_A C_N}} L_{IA} \left(kb_N \frac{z r^{\alpha_N}}{a_n P_A C_N} \right) \right] f_{\hat{R}_{N,0}}(r) dr, \quad (63)$$

and

$$\bar{F}_{\gamma_{f, near}^N} \approx \int_h^{R_f} \left[\sum_{k=1}^{m_N} (-1)^{k+1} \binom{m_N}{k} e^{-\frac{z}{a_m - a_n z} \frac{kb_N R_f^{\alpha_N} \sigma^2}{P_A C_N}} L_{IA} \left(\frac{z}{a_m - a_n z} \frac{kb_N R_f^{\alpha_N}}{P_A C_N} \right) \right] f_{\hat{R}_{N,0}}(r) dr. \quad (64)$$

Theorem 8. When the typical UE is associated with an ABS, and for the NLoS far UE case, the achievable ergodic rate can be expressed as

$$R_{far|NLoS} = \frac{1}{\ln 2} \int_0^{\infty} \frac{\bar{F}_{\gamma_{f, far}^N}(z)}{1+z} dz + \frac{1}{\ln 2} \int_0^{\frac{a_m}{a_n}} \frac{\bar{F}_{\gamma_{t, far}^N}(z)}{1+z} dz, \quad (65)$$

where

$$\bar{F}_{\gamma_{t, far}^N} \approx \int_{R_f}^{\infty} \left[\sum_{k=1}^{m_N} (-1)^{k+1} \binom{m_N}{k} e^{-\frac{z}{a_m - a_n z} \frac{kb_N r^{\alpha_N} \sigma^2}{P_A C_N}} L_{IA} \left(\frac{z}{a_m - a_n z} \frac{kb_N r^{\alpha_N}}{P_A C_N} \right) \right] f_{\hat{R}_{N,0}}(r) dr, \quad (66)$$

and

$$\bar{F}_{\gamma_{f, far}^N} \approx \int_{R_f}^{\infty} \left[\sum_{k=1}^{m_N} (-1)^{k+1} \binom{m_N}{k} e^{-kb_N \frac{z R_f^{\alpha_N} \sigma^2}{a_n P_A C_N}} L_{IA} \left(kb_N \frac{z R_f^{\alpha_N}}{a_n P_A C_N} \right) \right] f_{\hat{R}_{N,0}}(r) dr. \quad (67)$$

Theorem 9. The achievable ergodic rate of the NOMA enabled tier can be expressed as

$$R_A = \frac{A_L}{A_A} (R_{near|LoS} + R_{far|LoS}) + \frac{A_N}{A_A} (R_{near|NLoS} + R_{far|NLoS}). \quad (68)$$

Proof. Based on **Theorems 5-8**, and due to the fact that the typical UE is associated with an ABS, the result in (68) can be obtained.

VI. SIMULATION RESULTS

In this section, numerical results are provided to facilitate the performance evaluations of the proposed UAV-aided HetNets. 100,000 times Monte Carlo simulations are carried out to verify the accuracy of the analytical expressions. All the horizontal locations of ABSs and TBSs are distributed in a disc with radius 5×10^4 m. Other parameters are summarized in Table II.

TABLE II: Table of Parameters

Parameter	Value	Parameter	Value
λ_T	$10^{-5}/m^2$	λ_A	$0.2\lambda_T$
(a, b)	(12.08, 0.11)	h	200 m
R_B	220 m	R_f	$1.1h$
$(\alpha_N, \alpha_L, \alpha_T)$	(3, 2.5, 2)	(C_N, C_L, C_T)	(10, 3, 3) dB
(m_N, m_L, m_T)	(1, 2, 2)	(a_m, a_n)	(0.8, 0.2)
(P_T, P_A)	(20, 59) dBm	(σ_T^2, σ_A^2)	(-70, -104) dBm
N_T	4	(θ_a, θ_d)	$(\sqrt{3/N_T}, \sqrt{3/N_T})$
G_M	N_T	G_m	$\frac{\sqrt{N_T} - \frac{\sqrt{3}N_T \sin\left(\frac{3\pi}{2\sqrt{N_T}}\right)}{2\pi}}{\sqrt{N_T} - \frac{\sqrt{3} \sin\left(\frac{3\pi}{2\sqrt{N_T}}\right)}{2\pi}}$

First, we evaluate the association performance of the UAV-aided HetNets. In Fig. 2, for a given set of ABSs/TBSs densities, the solid curves and dashed curves are the association probability for TBSs and ABSs, respectively. It shows the association probability versus the altitude of ABSs, and the simulation results and analytical results match perfectly. We can observe that, at low altitudes, the probability that a typical UE is associated with an ABS is small due to the fact it experiences a large fraction of NLoS A2G links, which results in a large path loss. Then with the increase of the altitude of ABSs, the probability that a typical UE is associated with an ABS begins to increase. This is because the channel condition between the typical UE and the ABSs becomes better, i.e., the fraction of the LoS A2G links increases. When the altitude of the ABSs further increases, although most of the A2G links experience the LoS condition, the huge distance between the typical UE and the associated ABS will result in a non-negligible path loss. We can also notice that when the ratio of densities of ABSs and TBSs are fixed, a typical UE will tend to associate with a TBS when their densities are increased. This is rather intuitive due to the fact that the path loss exponent in mmWave transmissions is small.

We then investigate the coverage performance of the UAV-aided HetNets. Fig. 3 shows the

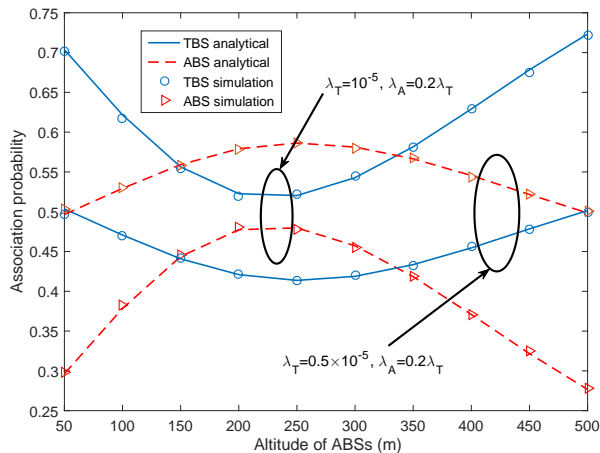


Fig. 2: Probability of association to an ABS/TBS versus altitude of ABSs for different densities coverage probability achieved by the typical UE when it is associated with a TBS. From the figure, we can observe that the analytical results match the simulation results well. Moreover, the analytical results are slightly larger than that of the simulation results. This is because we adopt the Alzer's Lemma to provide an approximation of a Gamma random variable when $m_T = 2$. We also plot the approximated analytical results shown in (40) in **Corollary 1**. The closed-form expression by adopting the Gaussian-Chebyshev quadrature has a relatively exact value compared with the simulation results. From Fig. 3, we also notice that due to the use of mmWave, the typical UE can achieve a large coverage probability, and with the increase of the number of antennas, the coverage probability will increase significantly even at a large SINR threshold.

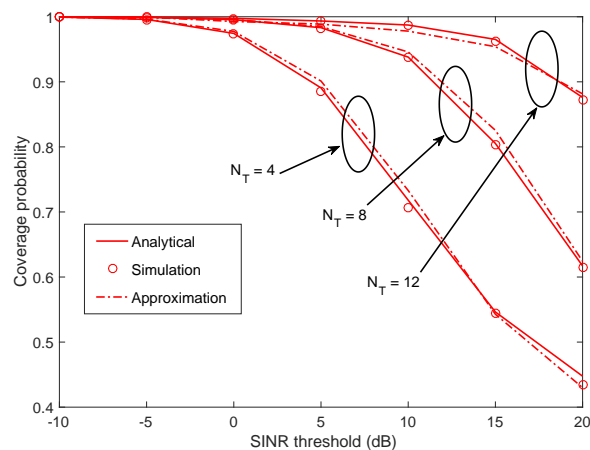


Fig. 3: TBS tier (mmWave tier) coverage probability versus SINR threshold, $h = 200$ m

Fig. 4 plots the coverage probability of a typical UE versus the altitude of ABSs when it is

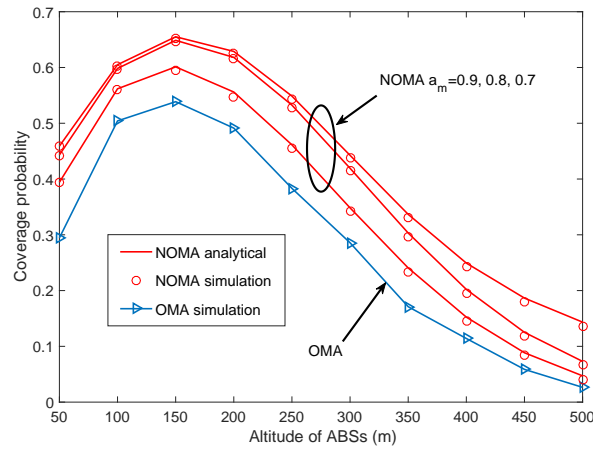


Fig. 4: NOMA enabled ABS tier coverage probability versus altitude of ABSs, $\epsilon_f = \epsilon_t = 0$ dB associated with an ABS both in the NOMA and OMA schemes. Note that the performance of the OMA scheme is only shown through the numerical approach, and it is adopted by dividing these two UEs in equal time/frequency slots. Similar to the results in Fig. 2, the coverage probability will first increase then decrease due to the A2G channel characteristics. We also demonstrate the superiority of NOMA over OMA when the power allocation factors are selected appropriately under some SINR threshold. It is worth mentioning that the power allocation between these two NOMA UEs can affect the coverage probability significantly. However, the optimization of the power allocation is beyond the scope of this paper.

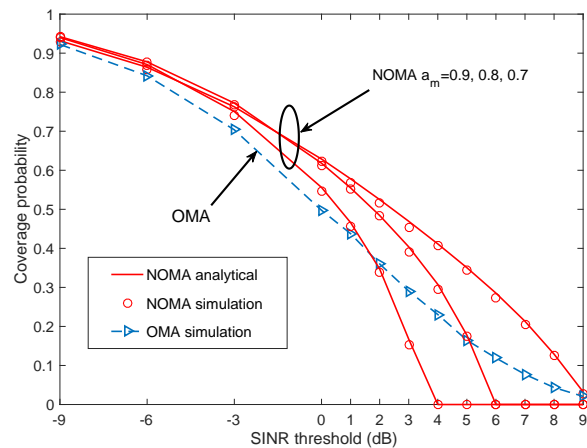


Fig. 5: NOMA enabled ABS tier coverage probability versus SINR threshold, $h = 200$ m

Next, Fig. 5 plots the coverage probability of a typical UE versus the SINR threshold when it is associated with an ABS both in the NOMA and OMA schemes. The results show that with

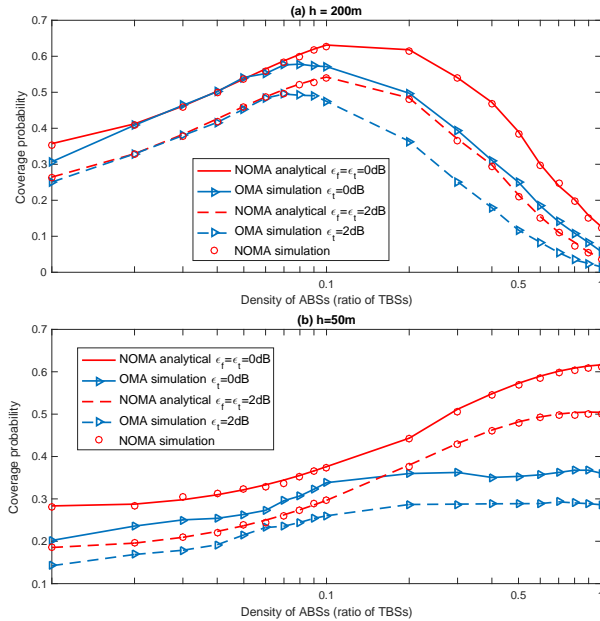


Fig. 6: NOMA enabled ABS tier coverage probability versus density of ABSs

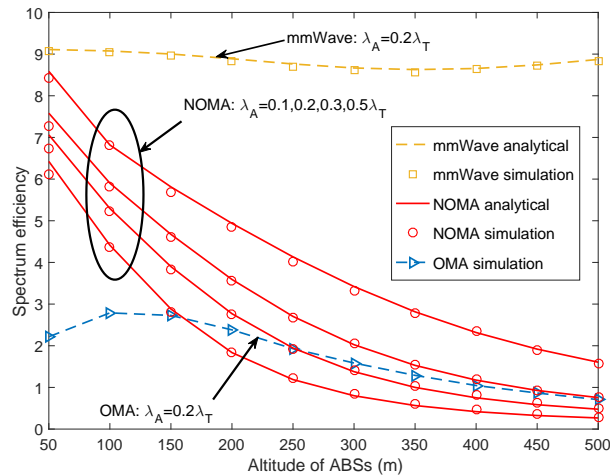


Fig. 7: Spectrum efficiency versus altitude of ABSs

the increase of the SINR threshold, the coverage probability decreases both for the NOMA and OMA schemes. It is also observed that the OMA scheme outperforms some particular NOMA scheme when the SINR threshold is large. This again demonstrates the importance of using power allocation. Besides, the coverage probability is always zero in the case of inappropriate power allocation factors given the target SINR threshold of the typical UE and the fixed UE, which coincides with **Remark 4**.

We then study the impact of network density on the coverage probability versus the density of

ABSs when the typical UE is associated with an ABS. Fig. 6 shows the coverage behaviour when the targeted SINR threshold is 0 dB and 2 dB with $h = 200$ m and $h = 50$ m, respectively. The density of TBSs is fixed as $10^{-5}/m^2$. It is observed that when $h = 200$ m, with the increase of the density of the ABSs, the coverage probability of the typical UE first increases and then decreases. This is because as we increase the density of the ABS, the probability that the ABSs can be selected as the serving BS will be increased. When the ABSs density is further increased, the interference from the non-serving ABSs will become larger, causing the decrease of the coverage probability. On the other hand, when $h = 50$ m, the coverage probability of the typical UE has an ascending trend. This is due to the fact that at low altitude interference is dominated by the NLoS signals. The results also show that under these settings, the NOMA scheme outperforms the OMA scheme, which again verifies the effectiveness of NOMA.

Finally, we verify the rate performance of the proposed UAV-aided HetNets. Fig. 7 shows the spectrum efficiency versus the altitude of ABSs. One can observe that due to the deployment of multiple antennas, mmWave can achieve a high spectrum efficiency regardless the change of ABSs altitude. In the NOMA scheme, the spectrum efficiency decreases with the increase of the altitude of ABSs, which indicates that the interference increases at a larger rate than the increase in the desired signals. Combined with the results in Fig. 2, we notice that with the increase of ABSs altitude, even the association probability connected to an ABS increases, the spectrum efficiency will decrease. This phenomenon reveals that the interference from the LoS ABSs should be carefully considered when we design the networks. On the other hand, in the OMA scheme, the spectrum efficiency will first increase and then decrease, due to at low altitude, the probability of LoS A2G transmissions is small. These results also verify the effectiveness of our proposed UAV-aided HetNets.

VII. CONCLUSIONS

A novel UAV-aided HetNets model consisting the NOMA-based ABSs and mmWave TBSs has been proposed to improve the coverage probability and spectrum efficiency in cellular networks. A flexible NOMA based UE association policy has been investigated. By using the tools from stochastic geometry, we derived the analytical expressions for the distance distributions given that the typical UE is associated with a TBS, a NLoS ABS or a LoS ABS. Additionally, new analytical expressions for association probability, coverage probability and spectrum efficiency

have also been derived for characterizing the performance of UAV-aided HetNets under the realistic A2G/G2G channels. Moreover, we provided the approximated expressions for the coverage probability and spectrum efficiency to simplify the analytical results. Finally, in the numerical results, we provided insights for the design of the HetNets i.e., the UEs tend to associate with the TBSs when the ABSs are deployed at low altitudes in a dense environment. We studied the impact of the ABSs altitude, network density, NOMA power allocation and SINR threshold in terms of the whole network performance. Analytical and simulated results demonstrated that terrestrial mmWave small cells can offer high capacity and the ABSs with NOMA are capable of achieving superior performance compared with the ABSs with OMA.

APPENDIX A: PROOF OF LEMMA 5

When the typical UE is associated to a LoS ABS, and there does not exist a TBS in $\mathcal{B}(0, R_B)$, $A_{L,1} = (1 - Q_T)\mathbb{P}(A_{L,1}^N) = (1 - Q_T)\mathbb{P}(\eta_L R_{L,0}^{-\alpha_L} > \eta_N R_{N,0}^{-\alpha_N})$

$$= (1 - Q_T) \left[\int_h^{l_{L,h}} f_{R_{L,0}}(r) dr + \int_{l_{L,h}}^\infty \exp\left(-2\pi\lambda_A \int_0^{\sqrt{\tau_{N|L}^2(r)-h^2}} x P_N(x) dx\right) f_{R_{L,0}}(r) dr \right], \quad (69)$$

where $A_{L,1}^N$ denotes the probability that the power received from the closest LoS ABS is stronger than that received from the closest NLoS ABS in the above scenario.

When there exists a TBS in $\mathcal{B}(0, R_B)$, the corresponding association probability is given by

$$A_{L,2} = Q_T Q_L \mathbb{P}(A_{L,2}^N) \mathbb{P}(A_{L,2}^T), \quad (70)$$

where $A_{L,2}^N$ and $A_{L,2}^T$ denote the probability that the power received from the closest LoS ABS is stronger than that received from the closest NLoS ABS and TBS in the above scenario, respectively. Then we have

$$\begin{aligned} \mathbb{P}(A_{L,2}^T) &= \frac{\mathbb{P}\left(R_{T,0} > \left(\frac{\eta_T}{\eta_L}\right)^{\frac{1}{\alpha_T}} R_{L,0}^{\frac{\alpha_L}{\alpha_T}} \mid R_{T,0} \leq R_B\right)}{Q_L Q_T} \\ &\stackrel{(a)}{=} \frac{\int_h^{l_{L,T}} [\mathbb{P}(R_{T,0} > \tau_{T|L}(r)) - (1 - Q_T)] f_{R_{L,0}}(r) dr}{Q_L Q_T} \\ &= \frac{\int_h^{l_{L,T}} \left[\exp\left(-\pi\lambda_T \tau_{T|L}^2(r)\right) - (1 - Q_T)\right] f_{R_{L,0}}(r)}{Q_L Q_T}, \end{aligned} \quad (71)$$

where (a) is due to the fact that there exists a TBS in $\mathcal{B}(0, R_B)$.

Similarly, we can derive the expression of $\mathbb{P}(A_{L,2}^N)$ shown in (26).

APPENDIX B: PROOF OF LEMMA 9

When the typical UE is associated with a TBS, the interference from the TBSs can be expressed

as $I_T = \sum_{x_{T,i} \in \Phi_T \cap \mathcal{B}(0, R_B) \setminus x_{T,0}} G_i P_T C_T R_{T,i}^{-\alpha_T} H_{T,i}$, then we have

$$\begin{aligned}
L_{I_T}(s) &= \mathbb{E}_{I_T} [e^{-sI_T}] \\
&\stackrel{(a)}{=} \mathbb{E}_{\Phi_T} \left[\prod_{x_{T,i} \in \Phi_T \cap \mathcal{B}(0, R_B) \setminus x_{T,0}} \mathbb{E}_{H_{T,i}} \left[e^{-sG_i P_T C_T R_{T,i}^{-\alpha_T} H_{T,i}} \right] \right] \\
&\stackrel{(b)}{=} \exp \left(-2\pi \lambda_T \sum_{j \in \{M, m\}} p_j \int_{R_{T,0}}^{R_B} \left(1 - \mathbb{E}_{H_{T,i}} \left[e^{-sG_j P_T C_T r^{-\alpha_T} H_{T,i}} \right] \right) r dr \right) \\
&\stackrel{(c)}{=} \exp \left(-2\pi \lambda_T \sum_{j \in \{M, m\}} p_j \int_{R_{T,0}}^{R_B} \left(1 - \left(1 + \frac{sP_T C_T G_j}{m_T r^{\alpha_T}} \right)^{-m_T} \right) r dr \right) \\
&\stackrel{(d)}{=} \exp \left(-2\pi \lambda_T \sum_{j \in \{M, m\}} \sum_{i=1}^{m_T} p_j \binom{m_T}{i} \left(\frac{sP_T C_T G_j}{m_T} \right)^i \int_{R_{T,0}}^{R_B} \frac{r^{-\alpha_T i + 1}}{\left(1 + \frac{sP_T C_T G_j}{m_T r^{\alpha_T}} \right)^{m_T}} dr \right) \\
&\stackrel{(e)}{=} \exp \left(\frac{-2\pi \lambda_T}{\alpha_T} \sum_{j \in \{M, m\}} \sum_{i=1}^{m_T} p_j \binom{m_T}{i} \left(\frac{sP_T C_T G_j}{m_T} \right)^{\frac{2}{\alpha_T}} (-1)^{\frac{2}{\alpha_T} - i + 1} \int_{t_{j,l}}^{t_{j,u}} \frac{t_j^{i - \frac{2}{\alpha_T} - 1}}{(1 - t_j)^{m_T}} dt_j \right), \tag{72}
\end{aligned}$$

where (a) is due to the properties of exponential terms, (b) is obtained by using probability generating functional (PGFL), (c) is obtained by computing the moment generating function of a Gamma random variable, (d) follows from the binomial theorem, and (e) is obtained by adopting $t_j = -\frac{sP_T C_T G_j}{m_T r^{\alpha_T}}$. Finally, from [27], $L_{I_T}(s)$ can be expressed as the form in (36).

APPENDIX C: PROOF OF LEMMA 11

The coverage probability of a typical UE when it is associated with a TBS is given by

$$\begin{aligned}
P_T^C &= \int_0^{R_B} \mathbb{P} \left(H_{T,0} \geq r^{\alpha_T} \frac{\nu_T}{G_M P_T C_T} (I_T + \sigma^2) \right) f_{\hat{R}_{T,0}}(r) dr \\
&\stackrel{(a)}{=} \int_0^{R_B} \left(\mathbb{E}_{I_T} \left[\exp(-m_T r^{\alpha_T} \varepsilon_T I_T) \cdot \sum_{k=0}^{m_T-1} \frac{(m_T r^{\alpha_T} \varepsilon_T (I_T + \sigma^2))^k}{k!} \right] \exp(-m_T r^{\alpha_T} \varepsilon_T \sigma^2) \right) f_{\hat{R}_{T,0}}(r) dr \\
&\stackrel{(b)}{=} \int_0^{R_B} \left(\sum_{k=0}^{m_T-1} \sum_{p=0}^k \binom{k}{p} \frac{r^{\alpha_T k} (m_T \varepsilon_T)^k}{k!} \exp(-m_T r^{\alpha_T} \varepsilon_T \sigma^2) (\sigma^2)^p \mathbb{E}_{I_T} [\exp(-m_T r^{\alpha_T} \varepsilon_T I_T) (I_T)^{k-p}] \right) f_{\hat{R}_{T,0}}(r) dr \\
&\stackrel{(c)}{=} \int_0^{R_B} \left(\sum_{k=0}^{m_T-1} \sum_{p=0}^k \binom{k}{p} \frac{r^{\alpha_T k} (m_T \varepsilon_T)^k}{k!} \exp(-m_T r^{\alpha_T} \varepsilon_T \sigma^2) (\sigma^2)^p \left[(-1)^{k-p} \frac{\partial^{k-p}}{\partial s^{k-p}} L_{I_T}(s) \right]_{s=m_T \varepsilon_T r^{\alpha_T}} \right) f_{\hat{R}_{T,0}}(r) dr, \tag{73}
\end{aligned}$$

where (a) is obtained from the CCDF of Gamma distribution, i.e. $\bar{F}_G(g) = \frac{\Gamma_u(m_T, m_T g)}{\Gamma(m_T)} = \exp(-m_T g) \sum_{k=0}^{m_T-1} \frac{(m_T g)^k}{k!}$, (b) follows from the binomial theorem, and (c) is from the fact that $\mathbb{E}_{I_T}[\exp(-s I_T) I_T^i] = (-1)^i \frac{\partial^i}{\partial s^i} L_{I_T}(s)$.

Since the above expression involves higher order derivatives of the Laplace transform which needs the aid of Faa Di Bruno's formula [28]. To reduce the high complexity, we adopt the Alzer's Lemma to give an approximation of a Gamma random variable [29], which is given by

$$\mathbb{P}(g < \tau) \approx [1 - e^{-b_T \tau}]^{m_T}, \quad (74)$$

where $b_T = m_T(m_T!)^{-\frac{1}{m_T}}$, then we have

$$\begin{aligned} P_T^C &= \int_0^{R_B} (1 - \mathbb{P}(H_{T,0} < r^{\alpha_T} \varepsilon_T (I_T + \sigma^2))) f_{\hat{R}_{T,0}}(r) dr \\ &\approx \int_0^{R_B} \left(1 - \mathbb{E}_{I_T} \left[\left(1 - e^{-b_T r^{\alpha_T} \varepsilon_T (I_T + \sigma^2)}\right)^{m_T} \right]\right) f_{\hat{R}_{T,0}}(r) dr \\ &\stackrel{(d)}{=} \int_0^{R_B} \left(\sum_{k=1}^{m_T} (-1)^{k+1} \binom{m_T}{k} e^{-k b_T r^{\alpha_T} \varepsilon_T \sigma^2} \mathbb{E}_{I_T} [e^{-k b_T r^{\alpha_T} \varepsilon_T I_T}] \right) f_{\hat{R}_{T,0}}(r) dr \\ &\stackrel{(e)}{=} \int_0^{R_B} \left(\sum_{k=1}^{m_T} (-1)^{k+1} \binom{m_T}{k} e^{-k b_T r^{\alpha_T} \varepsilon_T \sigma^2} L_{I_T}(k b_T r^{\alpha_T} \varepsilon_T) \right) f_{\hat{R}_{T,0}}(r) dr, \end{aligned} \quad (75)$$

where (d) follows from the binomial theorem, and (e) is obtained using the Laplace transform of interference.

REFERENCES

- [1] Y. Zeng, R. Zhang, and T. J. Lim, "Wireless communications with unmanned aerial vehicles: opportunities and challenges," *IEEE Commun Mag.*, vol. 54, no. 5, pp. 36–42, 2016.
- [2] Z. Xiao, P. Xia, and X.-G. Xia, "Enabling UAV cellular with millimeterwave communication: potentials and approaches," *IEEE Commun Mag.*, vol. 54, no. 5, pp. 66–73, 2016.
- [3] I. Bor-Yaliniz and H. Yanikomeroglu, "The new frontier in RAN heterogeneity: multi-tier drone-cells," *IEEE Commun Mag.*, vol. 54, no. 5, pp. 48–55, 2016.
- [4] A. Al-Hourani, S. Kandeepan, and S. Lardner, "Optimal LAP altitude for maximum coverage," *IEEE Wireless Commun. Lett.*, vol. 3, no. 6, pp. 569–572, Dec. 2014.
- [5] Y. Liu, Z. Qin, Y. Cai, Y. Gao, G. Y. Li, and A. Nallanathan, "UAV communications based on non-orthogonal multiple access," *IEEE Wireless Commun.*, vol. 26, no. 1, pp. 52–57, Feb. 2019.
- [6] T. Qi, W. Feng, and Y. Wang, "Outage performance of non-orthogonal multiple access based unmanned aerial vehicles satellite networks," *China Commun.*, vol. 15, no. 5, pp. 1–8, May 2018.
- [7] Z. Ding, P. Fan, and H. V. Poor, "Impact of user pairing on 5G nonorthogonal multiple-access downlink transmissions," *IEEE Trans. Veh. Technol.*, vol. 65, no. 8, pp. 6010–6023, Aug. 2016.
- [8] F. Boccardi, R. W. Heath, Jr., A. Lozano, T. L. Marzetta, and P. Popovski, "Five disruptive technology directions for 5G," *IEEE Commun. Mag.*, vol. 52, no. 2, pp. 74–80, Feb. 2014.

- [9] J. G. Andrews *et al.*, “What will 5G be?,” *IEEE J. Sel. Areas Commun.*, vol. 32, no. 6, pp. 1065–1082, Jun. 2014.
- [10] V. V. Chetlur and H. S. Dhillon, “Downlink coverage analysis for a finite 3-D wireless network of unmanned aerial vehicles,” *IEEE Trans. Commun.*, vol. 65, no. 10, pp. 4543–4558, Oct. 2017.
- [11] E. Turgut and M. C. Gursoy, “Downlink analysis in unmanned aerial vehicle (UAV) assisted cellular networks with clustered users,” *IEEE Access*, vol. 6, pp. 36313–36324, May 2018.
- [12] M. Alzenad and H. Yanikomeroglu, “Coverage and rate analysis for unmanned aerial vehicle base stations with LoS/NLoS propagation,” in *Proc. IEEE Glob. Commun. Conf. (Globecom) Workshops*, Abu Dhabi, UAE, Dec. 2018.
- [13] M. Alzenad and H. Yanikomeroglu, “Coverage and rate analysis for vertical heterogeneous networks (VHetNets),” *IEEE Trans. Wireless Commun.*, vol. 18, no. 12, pp. 5643–5657, Dec. 2019.
- [14] S. Sekander, H. Tabassum, and E. Hossain, “Multi-tier drone architecture for 5G/B5G cellular networks: challenges, trends, and prospects,” *IEEE Commun. Mag.*, vol. 56, no. 3, pp. 96–103, Mar. 2018.
- [15] D. Kim, J. Lee, and T. Q. S. Quek, “Multi-layer unmanned aerial vehicle networks: modeling and performance analysis,” *IEEE Trans. Wireless Commun.*, vol. 19, no. 1, pp. 325–339, Jan. 2020.
- [16] T. Hou, Y. Liu, Z. Song, X. Sun, and Y. Chen, “Exploiting NOMA for UAV communications in large-scale cellular networks,” *IEEE Trans. Commun.*, vol. 67, no. 10, pp. 6897–6911, Oct. 2019.
- [17] T. Hou, Y. Liu, Z. Song, X. Sun, and Y. Chen, “Multiple antenna aided NOMA in UAV networks: a stochastic geometry approach,” *IEEE Trans. Commun.*, vol. 67, no. 2, pp. 1031–1044, Feb. 2019.
- [18] H. Elshaer, M. N. Kulkarni, F. Boccardi, J. G. Andrews, and M. Dohler, “Downlink and uplink cell association with traditional macrocells and millimeter wave small cells,” *IEEE Trans. Wireless Commun.*, vol. 15, no. 9, pp. 6244–6258, Sep. 2016.
- [19] J. Park, S.-L. Kim, and J. Zander, “Tractable resource management with uplink decoupled millimeter-wave overlay in ultra-dense cellular networks,” *IEEE Trans. Wireless Commun.*, vol. 15, no. 6, pp. 4362–4379, Jun. 2016.
- [20] T. Bai and R. W. Heath, “Coverage and rate analysis for millimeter-wave cellular networks,” *IEEE Trans. Wireless Commun.*, vol. 14, no. 2, pp. 1100–1114, Feb. 2015.
- [21] J. G. Andrews, T. Bai, M. N. Kulkarni, A. Alkhatieb, A. K. Gupta, and R. W. Heath, “Modeling and analyzing millimeter wave cellular systems,” *IEEE Trans. Commun.*, vol. 65, no. 1, pp. 403–430, Jan. 2017.
- [22] K. Venugopal, M. C. Valenti, and R. W. Heath, “Device-to-device millimeter wave communications: interference, coverage, rate, and finite topologies,” *IEEE Trans. Wireless Commun.*, vol. 15, no. 9, pp. 6175–6188, Sep. 2016.
- [23] W. Yi, Y. Liu, E. Bodanese, A. Nallanathan, and G. K. Kargiannidis, “A unified spatial framework for UAV-aided mmWave networks,” *IEEE Trans. Commun.*, vol. 67, no. 12, pp. 8801–8817, Dec. 2018.
- [24] Y. Liu, Z. Qin, M. ElKashlan, Y. Gao, and L. Hanzo, “Enhancing the physical layer security of non-orthogonal multiple access in large-scale networks,” *IEEE Trans. Wireless Commun.*, vol. 16, no. 3, pp. 1656–1672, Mar. 2017.
- [25] Y. Liu, Z. Qin, M. ElKashlan, A. Nallanathan, and J. A. McCann, “Nonorthogonal multiple access in large-scale heterogeneous networks,” *IEEE J. Sel. Areas Commun.*, vol. 35, no. 12, pp. 2667–2680, Dec. 2017.
- [26] E. Hildebrand, *Introduction to Numerical Analysis*. New York, NY, USA: Dover, 1987.
- [27] I. S. Gradshteyn and I. M. Ryzhik, *Table of Integrals, Series and Products*, 6th ed. New York, NY, USA: Academic, 2000.
- [28] H. S. Dhillon, M. Kountouris, and J. G. Andrews, “Downlink MIMO HetNets: modeling, ordering results and performance analysis,” *IEEE Trans. Wireless Commun.*, vol. 12, no. 10, pp. 5208–5222, Oct. 2013.
- [29] H. Alzer, “On some inequalities for the incomplete Gamma function,” *Math. Comput.*, vol. 66, no. 218, pp. 771–778, 1997.